Journal of Alloys and Compounds 487 (2009) L12–L17

Contents lists available at ScienceDirect

Journal of Alloys and Compounds

journal homepage: www.elsevier.com/locate/jallcom

Letter

Structural and electrochemical performances of $Li_4Ti_{5-x}Zr_xO_{12}$ as anode material for lithium-ion batteries

Xing Li[a,b], Meizhen Qu[a], Zuolong Yu[a,*]

[a] Chengdu Institute of Organic Chemistry, Chinese Academy of Sciences, Chengdu 610041, China
[b] Graduate University of the Chinese Academy of Sciences, Beijing 100049, China

ARTICLE INFO

Article history:
Received 30 June 2009
Received in revised form 30 July 2009
Accepted 31 July 2009
Available online 8 August 2009

Keywords:
Lithium-ion battery
Spinel lithium titanate
Nano-particle
Doping
Rate capability

ABSTRACT

Zr-doped $Li_4Ti_5O_{12}$ in the form of $Li_4Ti_{5-x}Zr_xO_{12}$ (x = 0, 0.05, 0.1 and 0.2) was prepared by solid-state reaction in an air atmosphere. The dopant Zr partly entered the lattice structure of $Li_4Ti_5O_{12}$, and the excessive part existed as the impurity of ZrO_2. Zr-doping did not change the electrochemical reaction process of $Li_4Ti_5O_{12}$, but greatly affected its morphology and particle size. The particle size of the Zr-doped $Li_4Ti_5O_{12}$ sample was less than 100 nm and had less agglomeration. Zr-doping obviously improved the rate capability of $Li_4Ti_5O_{12}$ via the generation of small particle size and less agglomeration, however, a high amount of Zr-doping was adverse to the electrochemical performance probably due to much ZrO_2 impurity contained in the $Li_4Ti_5O_{12}$. $Li_4Ti_{4.9}Zr_{0.1}O_{12}$ exhibited a relatively good rate capability and cycling stability. At the charge–discharge rate of 5C, 10C and 20C, its discharge capacities were 143 mAh/g, 132 mAh/g and 118 mAh/g, respectively. After 100 cycles at 5C, it remained at 141 mAh/g.

1. Introduction

Recently, the spinel $Li_4Ti_5O_{12}$ has been demonstrated as a potential candidate for the anode material of lithium-ion batteries because of some of its unique characteristics [1–6]. It has good structural stability with an almost negligible volume change during the Li^+ insertion and extraction processes, which suggests virtually unlimited cycle life. It features a flat operating voltage of about 1.5 V vs. lithium, which is higher than the reduction potential of common electrolyte solvents. This voltage makes it safer than the presently used carbon-based anode materials because it is high enough to avoid the dangers of lithium plating that can occur at high-rate and/or low temperature operation [7].

Despite these mentioned advantages, however, $Li_4Ti_5O_{12}$ suffers from the problem of poor rate capability as a result of its low electronic conductivity. In order to improve the electronic conductivity of $Li_4Ti_5O_{12}$, there are two main methods. One is to improve its electronic conductivity by forming a composite of $Li_4Ti_5O_{12}$ and a conductive second phase such as Ag, C and polyacene [8–12]. Another is to synthesize $Li_4Ti_5O_{12}$ with ion doping. For example, doping $Li_4Ti_5O_{12}$ with Mg^{2+} or Al^{3+} on the Li^+ sites can increase the amount of mixing Ti^{3+}/Ti^{4+} as charge compensation and thus enhance its electronic conductivity [13,14]. In addition, doping Ta^{5+}, Br^{1-} into Ti^{4+} or O^{2-} sites can also increase the amount of mixing Ti^{3+}/Ti^{4+} as charge compensation [15,16]. Ion-doped $Li_4Ti_5O_{12}$ usually has relatively poor crystallinity according to the literatures, which suggests that the dopant has entered the lattice structure and resulted in lattice distortion. This process might affect the morphology and particle size of the product. However, little research has been attempted to investigate the morphology and particle size of $Li_4Ti_5O_{12}$ with ion doping. It has been reported that the high-rate charge/discharge properties of the $Li_4Ti_5O_{12}$ can be improved by reducing the grain sizes of the particles because small particles can reduce the distance for lithium-ion diffusion while providing a higher electrode/electrolyte contact surface area [17]. Therefore, selecting appropriate ion dopant to produce the $Li_4Ti_5O_{12}$ sample with small particle sizes might be an approach to improve its high-rate charge/discharge properties.

In the present work, we found that $Li_4Ti_5O_{12}$ with Zr^{4+}-doping yielded small particle sizes and low particle aggregates by using a solid-state reaction. Here, the effect of Zr-doping on the lattice structure, particle size, morphology and electrochemical characteristics of $Li_4Ti_5O_{12}$ was investigated. By the way of comparison, pristine $Li_4Ti_5O_{12}$ without the Zr-doping was also investigated.

2. Experimental

An undoped $Li_4Ti_5O_{12}$ sample was prepared by using a solid-state reaction from $CH_3COOLi{\cdot}2H_2O$ and TiO_2. Zr-doped $Li_4Ti_{5-x}Zr_xO_{12}$ (x = 0.05, 0.1 and 0.2) samples were also prepared by using a solid-state reaction with $CH_3COOLi{\cdot}2H_2O$, TiO_2 and $Zr(NO_3)_4{\cdot}5H_2O$. The undoped and doped $Li_4Ti_5O_{12}$ samples were named as 0Zr, 0.05Zr, 0.1Zr and 0.2Zr, respectively. A 0.2 mole% excessive $CH_3COOLi{\cdot}2H_2O$ was provided to compensate for Li volatilization during the high temperature heating. Firstly, the raw materials were dissolved in distilled water and stirred magnetically to form a well-mixed precursor slurry. The slurry was treated at 100 °C for about

* Corresponding author. Tel.: +86 28 85229790; fax: +86 28 85242280.
E-mail address: yzuolong@163.com (Z. Yu).

0925-8388/$ – see front matter © 2009 Elsevier B.V. All rights reserved.
doi:10.1016/j.jallcom.2009.07.176

10 h to became dried powder. The dried powder was then calcinated at 800 °C in air atmosphere for 12 h to obtain the final white powder of the samples.

The crystal structures of the samples were characterized by X-ray powder diffraction (XRD) measurement using the Philips X' Pert Pro MPD DY1219 with a Cu K_α radiation source. Particle morphologies and sizes of the samples were observed by scanning electronic microscopy (SEM FEI INSPECT-F). Specific surface areas of the samples were determined through nitrogen adsorption/desorption at −196 °C using a Builder SSA-4200 apparatus.

The electrochemical characterizations were measured by means of two-electrode coin-type half cells. To make the working electrodes, the synthesized samples were mixed with acetylene black (AB) and LA-132 binder with a weight ratio of 85:10:5 and ground into a paste. The prepared paste was spread onto aluminum foil using a doctor blade, with a 150 μm gap. The working electrodes were then dried at 100 °C in vacuum for 16 h before cell assembly. Li metal was used as the counter and reference electrode, and Celgard 2400 was the separator. The electrolyte was 1 M $LiPF_6$/EC:DEC:DMC (1:1:1 in volume). The cells were assembled in a glove box filled with high purity argon gas. Galvanostatic discharge–charge measurements were performed at constant cut-off voltages of 1–3 V at room temperature (25 °C). Cyclic voltammograms were recorded from 1 V to 3 V with a scan rate of 0.2 mV/s using MSTAT4+ Arbin Instruments. The AC impedance spectrum was measured by using a Solatron 1260 Impedance Analyzer in the frequency range 10^{-2} Hz to 10^5 Hz.

3. Results and discussion

The X-ray diffraction patterns of the synthesized $Li_4Ti_5O_{12}$ samples with and without Zr-doping are shown in Fig. 1. In order to correct for 2 theta error due to sample displacement in the XRD pattern measurement, the silicon was used as the internal standard. From Fig. 1, it can be seen that the main phase of all investigated samples is $Li_4Ti_5O_{12}$ with a cubic spinel structure, which suggests that the dopant Zr does not obviously change the structural characteristics of $Li_4Ti_5O_{12}$ during heat-treatment. However, as shown in Fig. 1, it can be observed that the XRD peak intensities of the samples decrease with the increase of the amount of Zr, which suggests that some dopant Zr has entered the lattice structure and that the Zr-doped $Li_4Ti_5O_{12}$ has relatively poor crystallinity. Fig. 1 also reveals that the diffraction peaks of the samples with the Zr-doping undergo a slight shift toward lower degrees. For clear observation, the peak positions of (1 1 1) planes of the samples are magnified and shown in Fig. 2. The lattice parameters of the samples obtained according to the Rietveld method are shown in Table 1. Therefore, it can be observed that the lattice parameter increases with the increased amount of Zr-doping, which should be ascribable to the substitution of some Zr for Ti sites and to the fact that the size of the Zr^{4+} (0.080 nm) ion is larger than that of Ti^{4+} (0.068 nm) ion.

Furthermore, Fig. 1 shows that ZrO_2 impurity peaks were detected in the curves of the 0.1Zr and 0.2Zr, and the peak intensities increase with the increased amount of doping Zr, which

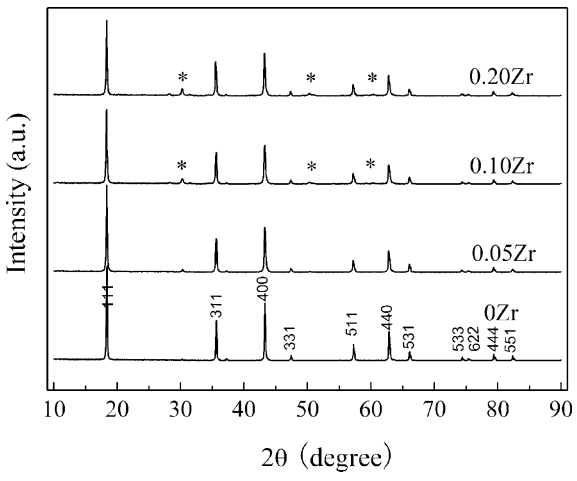

Fig. 1. X-ray diffraction patterns of synthesized $Li_4Ti_{5-x}Zr_xO_{12}$ (x = 0, 0.05, 0.1, 0.2) samples.

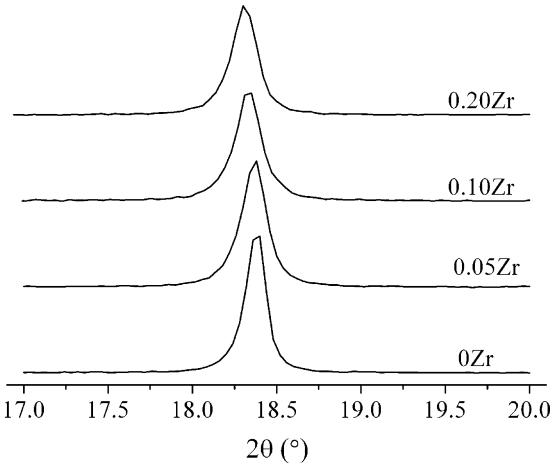

Fig. 2. Enlarged (1 1 1) peaks of synthesized $Li_4Ti_{5-x}Zr_xO_{12}$ samples doped with different Zr amounts: x = 0, 0.05, 0.1, 0.2.

Table 1
Lattice parameters of synthesized $Li_4Ti_{5-x}Zr_xO_{12}$ (x = 0, 0.05, 0.1, 0.2) samples.

Sample	a (Å)
0Zr	8.354
0.05Zr	8.356
0.10Zr	8.360
0.20Zr	8.361

indicates that some dopant Zr cannot enter the lattice structure of the $Li_4Ti_5O_{12}$ as the dopant amount increases. The ZrO_2 impurity peaks in the X-ray diffraction patterns are marked by an asterisk.

Fig. 3 shows the SEM pictures of the $Li_4Ti_5O_{12}$ samples with or without Zr-doping. Image A is the $Li_4Ti_5O_{12}$ sample without Zr-doping. Images B, C and D are the Zr-doped $Li_4Ti_{5-x}Zr_xO_{12}$ (x = 0.05, 0.1, 0.2, respectively) samples. Image A reveals that some of the particles of the $Li_4Ti_5O_{12}$ sample without Zr-doping form larger agglomerations, whereas images B–D show that the particles of the samples with varied amounts of doping have relatively less agglomerations.

Fig. 4 shows close-up SEM pictures of $Li_4Ti_{5-x}Zr_xO_{12}$ (x = 0, 0.05, 0.1, 0.2) samples. It can be observed that the $Li_4Ti_5O_{12}$ sample (image A) without Zr-doping has larger particle sizes than the samples (images B–D) with Zr-doping. The particle size as shown in image A is about 100–200 nm, while the sizes shown in images B–D are less than 100 nm. The BET surface areas of the samples with or without Zr-doping were determined by a nitrogen adsorption method, as shown in Table 2. It can be seen that the Zr-doped $Li_4Ti_{5-x}Zr_xO_{12}$ (x = 0.05, 0.1, 0.2) samples have larger BET surface areas than the $Li_4Ti_5O_{12}$ sample without Zr-doping and the BET surface areas of the Zr-doped samples increase with the increased doping amount of Zr. This means that the particle sizes of the doped samples decrease with the increased amount of Zr-doping.

The above results indicate that the $Li_4Ti_5O_{12}$ samples with varied amounts of Zr-doping have smaller particle sizes, less particle

Table 2
BET surface areas of synthesized $Li_4Ti_{5-x}Zr_xO_{12}$ (x = 0, 0.05, 0.1, 0.2) samples.

Sample	BET areas (m^2/g)
0Zr	4.025
0.05Zr	4.625
0.10Zr	5.145
0.20Zr	5.708

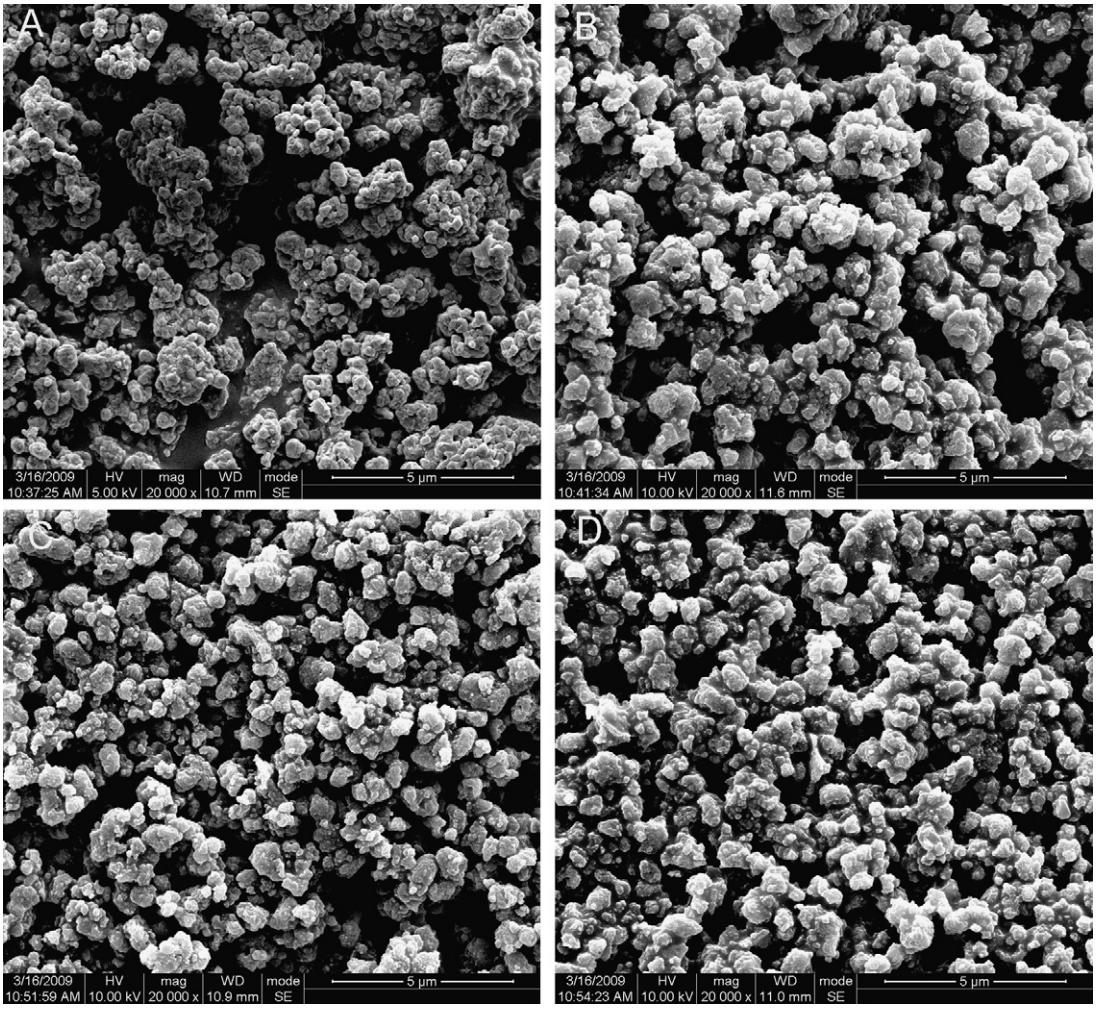

Fig. 3. SEM pictures of $Li_4Ti_{5-x}Zr_xO_{12}$ ($x = 0, 0.05, 0.1, 0.2$) samples.

agglomerations and larger surface areas than the sample without doping. This could be attributed to two reasons: (1) the dopant Zr that could enter the lattice structure of the $Li_4Ti_5O_{12}$, resulting in lattice distortion which hindered particle growth and agglomeration during heat-treatment; (2) part of the Zr dopant that could not enter the lattice structure of the $Li_4Ti_5O_{12}$ and constituted an impurity in the form of ZrO_2, which likewise hindered undesirable particle growth and agglomeration.

Fig. 5 shows the AC impedance spectra of the $Li_4Ti_{5-x}Zr_xO_{12}$ ($x = 0, 0.05, 0.1, 0.2$) electrodes, which were measured at the stable voltage of 1.55 V, respectively. AC impedance spectra are fitted using an equivalent circuit. In this equivalent circuit, R_s and R_{ct} are the solution resistance and charge transfer resistance, respectively. CPE is placed to represent the double layer capacitance and passivation film capacitance. W represents the Warburg impedance [18]. The plot of the real axis Z_{re} vs. the reciprocal square root of the lower angular frequencies $\omega^{-0.5}$ is illustrated in Fig. 6. The straight lines are attributed to the diffusion of the lithium ions into the bulk of the electrode materials, the so-called Warburg diffusion. From Fig. 6, we can obtain the value of Warburg impedance coefficient (σ_w). According to the following equations [19,20]:

$$Z_{re} = R_s + R_{ct} + \sigma_w.\omega^{-0.5}$$

$$D = 0.5\left(\frac{RT}{AF^2\sigma_w C}\right)^2$$

where R_{ct}, charge transfer resistance; R_s, solution resistance; ω, angular frequency in the low frequency region; D, diffusion coefficient; R, the gas constant; T, the absolute temperature; F, Faraday's constant; A, the area of the electrode surface; and C, molar concentration of Li^+ ions (moles cm^{-3}), the Li^+ ions diffusion coefficient D can be obtained. The impedance parameters are recorded in Table 3.

From Table 3, it can be seen that the Zr-doped $Li_4Ti_{5-x}Zr_xO_{12}$ ($x = 0.05, 0.1, 0.2$) electrodes have better electronic conductivity and ionic conductivity than the $Li_4Ti_5O_{12}$ electrode without Zr-doping. This should be ascribed to the fact that the Zr-doped $Li_4Ti_{5-x}Zr_xO_{12}$ ($x = 0.05, 0.1, 0.2$) samples have smaller particle sizes and less particle agglomerations than the $Li_4Ti_5O_{12}$ sample without Zr-doping. Furthermore, among the Zr-doped electrodes, it can be seen that the 0.1Zr electrode has the best electronic conductivity and ionic conductivity as shown in Table 3, which indicates that the selection of an appropriate amount of Zr dopant is important. This result might be attributed to the impurity of ZrO_2. As mentioned above, with the increased amount of the Zr-doping, part of the dopant

Table 3
The impedance parameters of the $Li_4Ti_{5-x}Zr_xO_{12}$ ($x = 0, 0.05, 0.1, 0.2$) electrodes.

Sample	R_s (Ω)	R_{ct} (Ω)	σ_w (Ω $cm^2/s^{0.5}$)	D (cm^2/s)
0Zr	3.2	165.9	383.5	9.61E−13
0.05Zr	2.6	124.1	180.3	4.40E−12
0.10Zr	2.0	99.6	147.5	6.58E−12
0.20Zr	2.7	135.3	234.0	2.61E−12

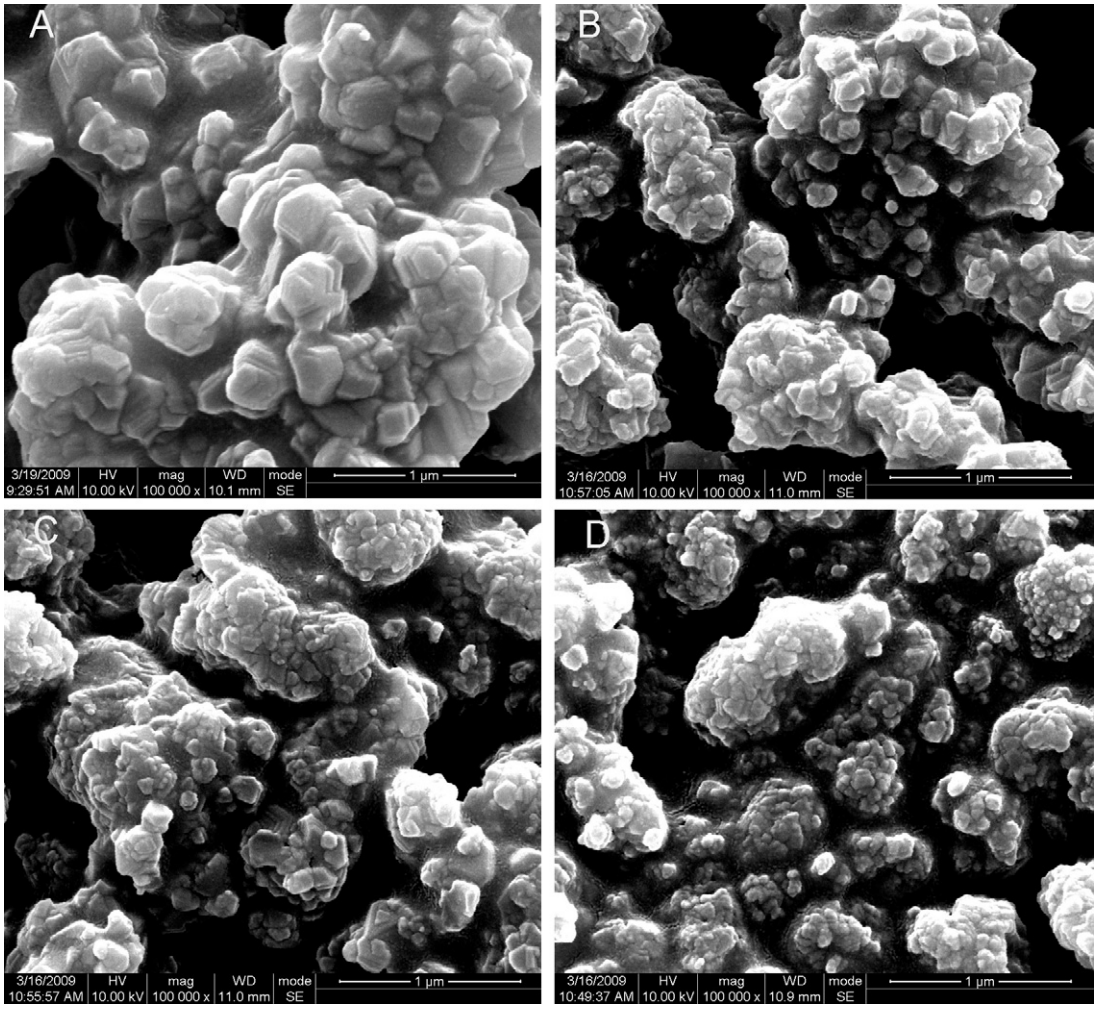

Fig. 4. Close-up SEM pictures of $Li_4Ti_{5-x}Zr_xO_{12}$ (x = 0, 0.05, 0.1, 0.2) samples.

could not enter the lattice structure of the $Li_4Ti_5O_{12}$. This part constituted an impurity in the form of ZrO_2, as detected by the X-ray diffraction patterns. ZrO_2 has high dielectric constant [21], which probably has lower lithium ionic conductivity and electronic conductivity than $Li_4Ti_5O_{12}$ and thus impedes the transportation of Li-ions and electrons. Therefore, when the amount of Zr-doping is high, there would be much ZrO_2 contained in the product, which is adverse to the conductivity of $Li_4Ti_5O_{12}$.

Fig. 7 shows the cyclic performance of the $Li_4Ti_{5-x}Zr_xO_{12}$ (x = 0, 0.05, 0.1, 0.2) samples at different rates from 0.5C, 1.0C, 3.0C, 5.0C, 10.0C to 20.0C. The charge–discharge processes of the samples were taken for 10 cycles at 0.5C, 1.0C, 3.0C, 5.0C, 10.0C and 20.0C, respectively. It can be observed that the undoped sample 0Zr exhibited a high discharge capacity and good cycling stability at 0.5C and 1.0C. At 0.5C, its initial discharge capacity was 166 mAh/g, and at 1.0C, its

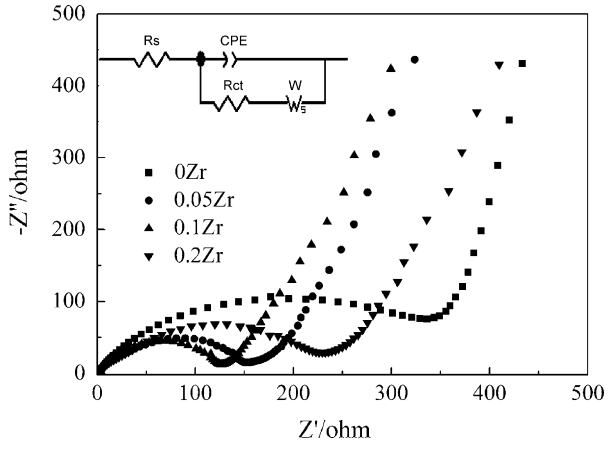

Fig. 5. AC impedance spectra of the $Li_4Ti_{5-x}Zr_xO_{12}$ (x = 0, 0.05, 0.1, 0.2) electrodes at the voltage of 1.55 V.

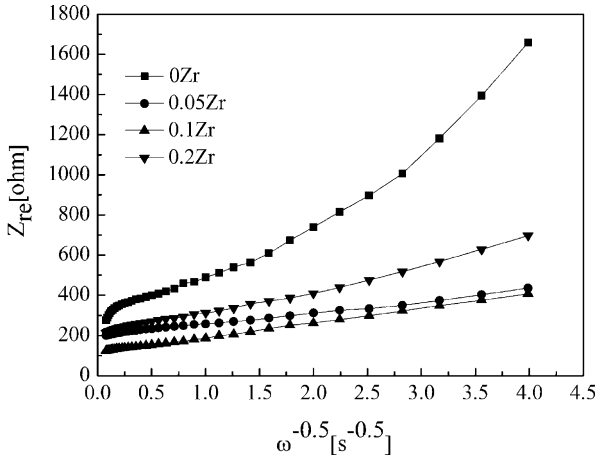

Fig. 6. Relationship between real impedance with the low frequencies for the $Li_4Ti_{5-x}Zr_xO_{12}$ (x = 0, 0.05, 0.1, 0.2) electrodes.

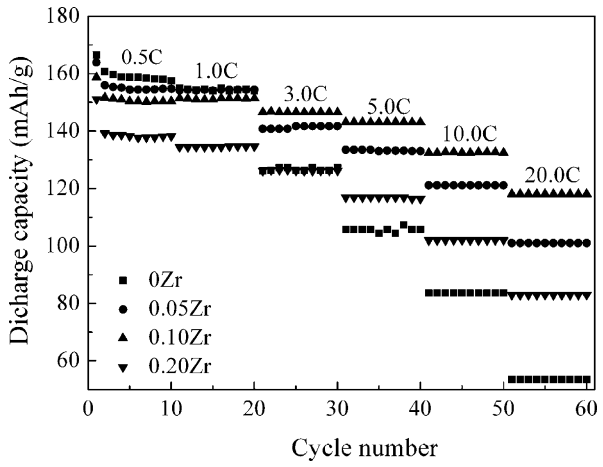

Fig. 7. Cyclic performance of the $Li_4Ti_{5-x}Zr_xO_{12}$ ($x = 0, 0.05, 0.1, 0.2$) samples at different rates: 1st–10th cycles at 0.5C, 11th–20th at 1.0C, 21th–30th at 3.0C, 31th–40th at 5.0C, 41th–50th at 10.0C, 51th–60th at 20.0C.

capacity remained at 155 mAh/g. With the rate increase, however, its capacity quickly decreased. At 3.0C, its capacity was 126 mAh/g; at 10.0C, it was 83 mAh/g; and at 20.0C, its capacity remained at only 53 mAh/g. In contrast, the doped samples 0.05Zr, 0.1Zr and 0.2Zr displayed relatively low discharge capacity at 0.5C and 1.0C. At 0.5C, their capacities were 164 mAh/g, 159 mAh/g and 151 mAh/g, respectively; and at 1.0C they were 154 mAh/g, 151 mAh/g and 134 mAh/g. As shown in Fig. 7, however, the discharge capacities of the doped samples manifested less capacity degradation with the rate increase than the undoped sample. For example, at 3.0C, the capacities of the doped samples 0.05Zr, 0.1Zr and 0.2Zr were 141 mAh/g, 146 mAh/g, and 126 mAh/g, respectively; at 10.0C, they were 121 mAh/g, 132 mAh/g and 102 mAh/g; and at 20.0C, they still remained at 101 mAh/g, 118 mAh/g and 83 mAh/g. For clear observation, the initial discharge capacities of the samples 0Zr, 0.05Zr, 0.1Zr and 0.2Zr as a function of the charge/discharge rates are shown in Fig. 8. These results indicate that Zr-doping impairs the capacity of the $Li_4Ti_5O_{12}$ at low rates, but can obviously enhance its rate capability. This could be ascribed to Zr-doping samples having smaller particle sizes and less particle agglomerations than the undoped $Li_4Ti_5O_{12}$. Smaller particles and less particle agglomerations could reduce the distance for lithium-ion diffusion and provide for a higher electrode/electrolyte contact surface area, which improve the electronic conductivity of the electrodes, resulting in good rate capability. It is worth noting that, as shown in Fig. 7, the 0.1Zr sample has the best rate capability of all the doped samples, which indicates that the $x = 0.1$ dopant amount is appropriate. These results are in good agreement with the AC impedance spectra of the $Li_4Ti_{5-x}Zr_xO_{12}$ ($x = 0, 0.05, 0.1, 0.2$) electrodes mentioned above.

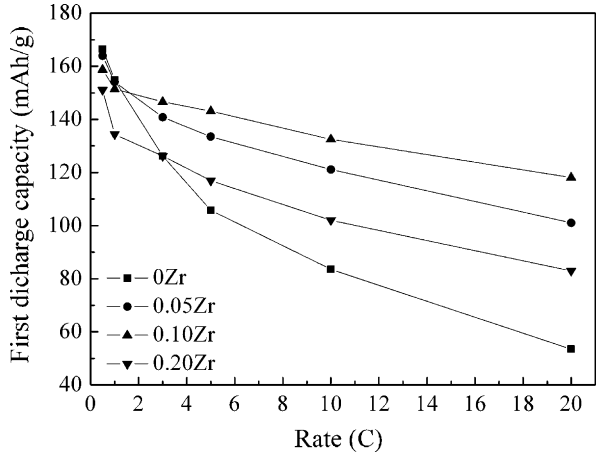

Fig. 8. Discharge capacities of the samples 0Zr, 0.05Zr, 0.1Zr and 0.2Zr as a function of the charge/discharge rates.

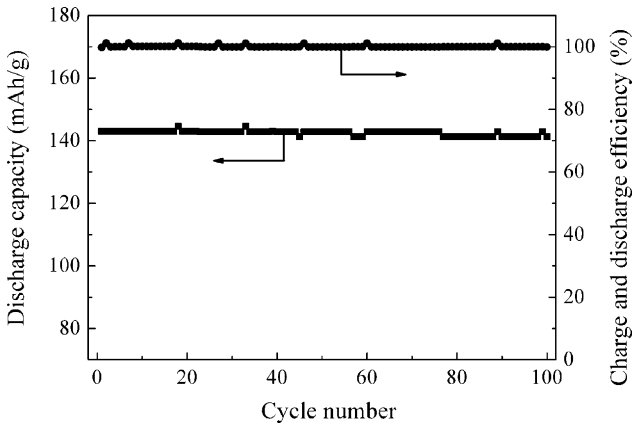

Fig. 9. Cyclic performance of the 0.1Zr sample at 5.0C.

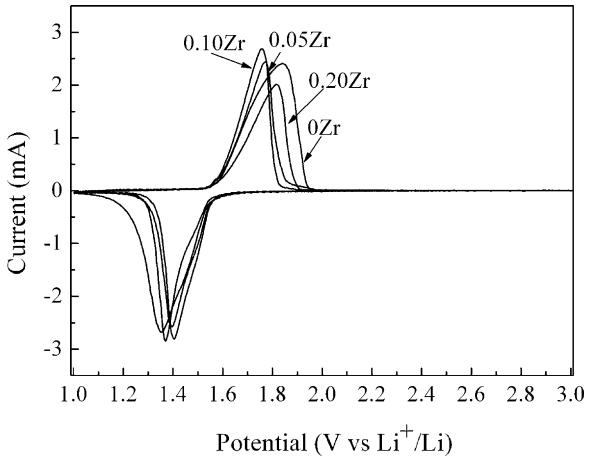

Fig. 10. Cyclic voltammograms of the samples 0Zr, 0.05Zr, 0.1Zr and 0.2Zr. Scan rate: 0.2 mV/s.

For evaluating the cycling stability of the 0.1Zr sample, it was further charge–discharged at a current rate of 5C for another 100 cycles after the 60 cycles electrochemical tests performed at 0.5C, 1.0C, 3.0C, 5.0C, 10.0C and 20.0C. This is shown in Fig. 9. It can be observed that the 0.1Zr sample shows a stable cycle life. The initial discharge capacity of the sample was 143 mAh/g, and even after 100 charge–discharge cycles, its capacity remained at 141 mAh/g. Furthermore, as Fig. 9 shows, the charge and discharge efficiency remained almost at 100%.

Table 4
Potential differences between anodic and cathodic peaks for the synthesized $Li_4Ti_5O_{12}$ samples doped with different amounts of Zr.

Sample	Anodic peak (V)	Cathodic peak (V)	Difference between anodic and cathodic peak (V)
0Zr	1.844	1.354	0.490
0.05Zr	1.769	1.387	0.382
0.10Zr	1.756	1.404	0.352
0.20Zr	1.819	1.370	0.449

Cyclic voltammograms of the electrodes 0Zr, 0.05Zr, 0.1Zr and 0.2Zr at a scan rate of 0.2 mV/s between 1 V and 3 V are shown in Fig. 10. It is shown that all the investigated electrodes have similar redox peaks, suggesting that Zr-doping does not change the electrochemical reaction process of $Li_4Ti_5O_{12}$. The potential differences between anodic and cathodic peaks for the $Li_4Ti_{5-x}Zr_xO_{12}$ ($x = 0$, 0.05, 0.1, 0.2) electrodes are shown in Table 4. It can be observed that the Zr-doped $Li_4Ti_{5-x}Zr_xO_{12}$ ($x = 0.05$, 0.1, 0.2) electrodes have lower potential differences than the pristine $Li_4Ti_5O_{12}$ (0Zr) and that the 0.1Zr electrode has the smallest potential difference among the doped samples. These indicate that Zr-doping is favorable for reducing the electrode polarization, but that too high an amount of doping is disadvantageous.

4. Conclusions

The structure and electrochemical characteristics of the Zr-doped $Li_4Ti_5O_{12}$ in the form of $Li_4Ti_{5-x}Zr_xO_{12}$ ($x = 0$, 0.05, 0.1, 0.2) were investigated in the present study. The Zr-doped $Li_4Ti_5O_{12}$ samples had smaller particle sizes and less particle agglomerations than the pristine $Li_4Ti_5O_{12}$ and Zr-doping did not change the electrochemical reaction process of $Li_4Ti_5O_{12}$. The dopant Zr partly entered the lattice structure of $Li_4Ti_5O_{12}$ as the doping amount increased, and thus constituted an impurity in the form of ZrO_2. The ZrO_2 impurity probably has lower lithium ionic conductivity and electronic conductivity as compared with $Li_4Ti_5O_{12}$, which was disadvantageous to the electrochemical characteristics. The Zr dopant can yield smaller particle sizes and less particle agglomerations that are favorable to the electrochemical performances of $Li_4Ti_5O_{12}$, but also it might impair it caused by the impurity of ZrO_2. Therefore, there was an optimum amount for Zr-doping. From the overall performance point of view, the 0.1Zr sample exhibited the best rate capability.

Acknowledgements

This work was carried out with financial support from Ministry of Science and Technology of the People's Republic of China (No. 2006CB932703) and Key Item of knowledge Innovation Project of Chinese Academy of Science (No. KJCX2-YW-M01).

References

[1] A. Guerfi, S. Sévigny, M. Lagacé, P. Hovington, K. Kinoshita, K. Zaghib, J. Power Sources 119–121 (2003) 88.
[2] M. Venkateswarlu, C.H. Chen, J.S. Do, C.W. Lin, T.C. Chou, B.J. Hwang, J. Power Sources 146 (2005) 204.
[3] J.L. Allen, T.R. Jow, J. Wolfenstine, J. Power Sources 159 (2006) 1340.
[4] J.J. Huang, Z.Y. Jiang, Electrochim. Acta 53 (2008) 7756.
[5] S.Y. Yin, L. Song, X.Y. Wang, M.F. Zhang, K.L. Zhang, Y.X. Zhang, Electrochim. Acta 54 (2009) 5629.
[6] T. Yuan, K. Wang, R. Cai, R. Ran, Z.P. Shao, J. Alloys Compd. 477 (2009) 665.
[7] J. Wolfenstine, U. Lee, J.L. Allen, J. Power Sources 154 (2006) 287.
[8] S.H. Huang, Z.Y. Wen, J.C. Zhang, Z.H. Gu, X.H. Xu, Solid State Ionics 177 (2006) 851–855.
[9] R. Dominko, M. Gaberscek, U. Bele, D. Mihailovic, J. Jamnik, J. Eur. Ceram. Soc. 27 (2007) 909–913.
[10] L. Yang, L. Gao, J. Alloys Compd. (2009), doi:10.1016/j.jallcom.2009.05.151.
[11] H. Liu, Y. Feng, K. Wang, J.Y. Xie, J. Phys. Chem. Solids 69 (2008) 2037–2040.
[12] H.Y. Yu, X.F. Zhang, A.F. Jalbout, X.D. Yan, X.M. Pan, H.M. Xie, R.S. Wang, Electrochim. Acta 53 (2008) 4200–4204.
[13] C.H. Chen, J.T. Vaughey, A.N. Jansen, D.W. Dees, A.J. Kahaian, T. Goacher, M.M. Thackeray, J. Electrochem. Soc. 148 (2001) A102.
[14] H.L. Zhao, Y. Li, Z.M. Zhu, J. Lin, Z.H. Tian, R.L. Wang, Electrochim. Acta 53 (2008) 7079.
[15] J. Wolfenstine, J.L. Allen, J. Power Sources 180 (2008) 582–585.
[16] Y.L. Qi, Y.D. Huang, D.Z. Jia, S.J. Bao, Z.P. Guo, Electrochim. Acta 54 (2009) 4772–4776.
[17] L. Cheng, H.J. Liu, J.J. Zhang, H.M. Xiong, Y.Y. Xia, J. Electrochem. Soc. 153 (2006) A1472.
[18] A.Y. Shenouda, K.R. Murali, J. Power Sources 176 (2008) 332–339.
[19] A.Y. Shenouda, H.K. Liu, J. Power Sources 185 (2008) 1386–1391.
[20] A.Y. Shenouda, H.K. Liu, J. Alloys Compd. 477 (2009) 498–503.
[21] T.S. Kalkur, Y.C. Lu, Thin Solid Films 207 (1992) 193.